Impact of the Universe's expansion rate on constraints on modified growth of structure

Jaime Ruiz-Zapatero,* David Alonso, Pedro G. Ferreira, and Carlos Garcia-Garcia
Astrophysics, University of Oxford, DWB, Keble Road, Oxford OX1 3RH, United Kingdom

(Received 20 July 2022; accepted 19 September 2022; published 21 October 2022)

In the context of modified gravity, at the linear level, the growth of structure in the Universe will be affected by modifications to the Poisson equation and by the background expansion rate of the Universe. It has been shown that these two effects lead to a degeneracy which must be properly accounted for if one is to place reliable constraints on new forces on large scales or, equivalently, modifications to general relativity. In this paper we show that current constraints are such that assumptions about the background expansion have little impact on constraints on modifications to gravity. We do so by considering the background of a flat, Λ cold dark matter universe, a universe with a more general equation of state for the dark energy, and finally, a general, model-independent, expansion rate. We use Gaussian processes to model modifications to Poisson's equation and, in the case of a general expansion rate, to model the redshift-dependent Hubble rate. We identify a degeneracy between modifications to Poisson's equation and the background matter density, Ω_M, which can only be broken by assuming a model-dependent expansion rate. We show that, with current data, the constraints on modifications to the Poisson equation via measurements of the growth rate range between 10–20% depending on the strength of our assumptions on the Universe's expansion rate.

DOI: 10.1103/PhysRevD.106.083523

I. INTRODUCTION

The growth of structure in the Universe is a sensitive probe of fundamental physics [1,2]. It is driven by gravitational collapse but is also sensitive to additional forces which may be undetectable on smaller, laboratory scales. It has been shown that measurements of the *rate* of growth of structure can be used to test gravity and constrain, as yet, elusive fifth forces [3].

To be specific, the motion of matter in the Universe can, in general, be subjected to an effective force, $\vec{F}_{\rm eff}$ of the form

$$\vec{F}_{\rm eff} = -\vec{\nabla}\Psi_N - \vec{\nabla}\Psi_5. \tag{1}$$

Here, Ψ_N is the Newtonian potential and Ψ_5 is the potential for a possible long-range force that coexists with gravity on large scales. The properties of Ψ_5 may depend on the state of the Universe (e.g., its expansion rate or the fractional energy densities of its different constituents) or even on local environmental properties [4,5]. Thus Ψ_5/Ψ_N will, generally, be a function of space and time.

If we restrict ourselves to purely long-range forces with no environmental dependence, we can define a generalized Newtonian potential, $\Psi \equiv \Psi_5 + \Psi_N$. In an expanding Universe with scale factor, a, Ψ satisfies a Newton-Poisson equation on subhorizon scales

$$\nabla^2\Psi = 4\pi G\mu a^2\bar{\rho}\delta, \tag{2}$$

where G is Newton's constant, $\bar{\rho}$ is the background energy density of nonrelativistic matter, and δ is the density contrast. We will assume μ is a function of time only although, in certain scenarios, it can be scale dependent. The relative amplitude of the new force, at any moment in time, is given by $\mu - 1$.

From the linearized Newton-Poisson, continuity and Euler equations one can derive an evolution equation for the growth rate of structure, $f \equiv d\ln\delta/d\ln a$, given by

$$f' + f^2 + \left(1 + \frac{d\ln aH}{d\ln a}\right) f = \frac{3}{2}\mu\Omega_M(a), \tag{3}$$

where a prime denotes a derivative with respect to $\ln a$, H is the Hubble rate and $\Omega_M(z)$ is the fractional energy density in matter as a function of redshift [1,6,7]. Thus, as we can see, the evolution of f depends on μ. This means that, in theory, one can use measurements of the growth rate to constrain the presence of fifth forces.

The situation is, of course, more complex. The evolution of the growth rate depends on the evolution of H and $\Omega_M(a)$. The latter quantity depends, through the Einstein field equations, on $H(a)$ so that

$$\Omega_M(a) = \frac{\Omega_M(0)H_0^2}{a^3H^2}. \tag{4}$$

*jaime.ruiz-zapatero@physics.ox.ac.uk

Thus, measurements of the growth rate can be used to place constraints on the time evolution of μ and H, and on the fractional matter density today, $\Omega_M(0)$ (for ease of notation, we will now refer to it as Ω_M with no argument). But this means that constraints on these various quantities are intertwined and, unless we have independent methods for pinning down H and Ω_M, they will hamper our ability to determine μ.

This degeneracy between μ and the expansion history (encapsulated in H, for example) was discussed in Ref. [8]. There, it was shown that there is a degeneracy between $\gamma \equiv \partial \ln f / \partial \ln \Omega_M$ and the equation of state of the dark energy component, $w \equiv P_{\rm DE}/\rho_{\rm DE}$, where $\rho_{\rm DE}$ ($P_{\rm DE}$) is the energy density (pressure) of the substance responsible for the accelerated expansion of the Universe at late times (the dark energy). In Ref. [7], explicit expressions for the degeneracy between μ and w were found using the linear response approach.

Most attempts to constrain $\mu(z)$ have assumed a Universe in which the accelerated expansion at late times is driven by a cosmological constant, i.e., the Λ cold dark matter (ΛCDM) model [9–11]. A further assumption is that $\mu(z)$ can be modeled in terms of a simple function with one (or at most two) parameters [9]. In a few cases, a more general form for $\mu(z)$ has been assumed with a few independent values at different redshifts (for a notable example see Ref. [10]). Alternatively, model-specific time dependences for $\mu(z)$ have been assumed arising from theoretical arguments, either from the effective field theory of dark energy [12,13] or from choices for the underlying model of gravity (such as shift-symmetric scalar-tensor gravity and its extensions [14]). Most of these attempts at constraining $\mu(z)$ have sidestepped the issue of the degeneracy described above although we highlight Ref. [15] and its attempt to obtain model-independent constraints.

In this paper we explore how current constraints on μ are affected by our assumptions about the expansion rate of the Universe. In particular, we will see how more or less restrictive assumptions about the parametric form of $H(z)$ impact the uncertainty with which we can determine $\mu(z)$. In the limit in which we do not assume a parametrized form for $H(z)$ we show that a fundamental degeneracy between Ω_M and $\mu(z)$ manifests itself and, in that regime, we must resign ourselves to constraining the combination $\Omega_M\mu(z)$.

The structure of this paper is as follows. In Sec. II we present the main method of this paper, i.e., the use of a Gaussian process as a model-independent parametrization of $\mu(z)$. In Sec. III we discuss how to interpret said Gaussian process. In Sec. IV we describe the cosmological observables and the associated data sets which we use to find the constraints in this paper. In Sec. V we present our constraints on $\mu(z)$ and how they depend on what we assume as a model for the background evolution; we focus on ΛCDM and its extension wCDM, in which we assume an (possibly time-varying) arbitrary equation of state, w. In Sec. VI we completely free the background evolution and model $H(z)$ as a Gaussian process. This gives rise to a strong degeneracy between Ω_M and $\mu(z)$ and we can only constraint $\tilde{\mu}(z) = \Omega_M\mu(z)$. In Sec. VII we discuss both our finding about the role of Gaussian processes in cosmological analysis and the constraints we find on $\mu(z)$.

II. GAUSSIAN PROCESS FOR $\mu(z)$

The goal of this work is to quantify the uncertainty in our knowledge of $\mu(z)$. The quality of this constraint will depend on both the quality of the data and the assumptions we make about the underlying cosmology through the expansion rate. We want to assume that we have no prior knowledge of the time dependence of $\mu(z)$, apart from the fact that it is relatively smooth. Thus, we choose to model $\mu(z)$ as a Gaussian process (GP).

GPs have been extensively used in astrophysics as tools to model different quantities in an agnostic way [16–28]. Fundamentally, a GP is a collection of random variables (nodes), each of them sampled from a multivariate Gaussian distribution with a nondiagonal covariance [29]. Thus a GP $g(\mathbf{x})$ where $\mathbf{x}$ is an arbitrary vector representing the position of the nodes, is fully specified by a mean function $m(\mathbf{x}) \equiv \mathcal{E}[g(\mathbf{x})]$ (where $\mathcal{E}[\cdots]$ is the expectation value over the ensemble) and a covariance function $k(\mathbf{x},\mathbf{x}') \equiv \mathcal{E}[(g(\mathbf{x}) - m(\mathbf{x}))(g(\mathbf{x}') - m(\mathbf{x}'))]$. In combination, the mean and covariance functions determine the statistical properties of the random variables that define the family of shapes that the GP can take. In our case, we chose $\mu(a) = 1$ as the mean of our GP since this is the value corresponding to general relativity (GR). For the covariance function, we choose a square exponential covariance function, defined as

$$k[g(x), g(x')] = \eta^2 \exp \frac{|x - x'|^2}{2l^2}, \tag{5}$$

where η is the amplitude of the oscillations around the mean and l is the correlation length between the GP realizations. This decision was made based on the fact that the square exponential is a computationally inexpensive and infinitely differentiable kernel, appropriate for modeling smooth fluctuations around the mean of the GP.

Given a likelihood $\mathcal{L}(\mathbf{y}|\mathbf{x},\boldsymbol{\sigma})$ for a set of data points $\mathbf{y}$, with a set of errors $\boldsymbol{\sigma}$, and a set of random variables $\mathbf{x}$, a GP can be employed as a prior over all the possible families of functions used to fit the observations. Observations can then be used to inform the GP posterior (i.e. the statistical properties of the ensemble of random variables), $\mathcal{P}(g(\mathbf{x})|\mathbf{y},\boldsymbol{\sigma})$, which determines the family of functions most consistent with the data.

Since we do not have direct measurements of $\mu(z)$, we have to infer it from measurements of the growth rate.

However, as one can see from Eq. (3), $f\sigma_8$ also depends on $H(z)$ and Ω_M. Thus, we must jointly determine $\mu(z)$, $H(z)$ and Ω_M in terms of measurements of $f\sigma_8$ and $H(z)$, or derived quantities such as the comoving $[D_M(z)]$, luminosity $[D_L(z)]$ or the angular diameter $[D_A(z)]$ distances, which are related to $H(z)$ via

$$(1+z)D_A = \frac{D_L}{1+z} = D_M = \int_0^z \frac{dz'}{H(z')}. \tag{6}$$

In summary, as we can see from Eqs. (3) and (6), computing predictions for our observables will involve a nonlinear, nonlocal mapping between the quantities we are interested in $[\mu(z), \Omega_M, H(z)\ldots]$ and the data. For example, a measurement of $f\sigma_8$ at a particular redshift, z, constrains the *history* of μ up until that redshift and not only the value of μ *at* that redshift.

The fact that the variables of our model are not linearly related to our data has, nonetheless, strong implications. Namely, we will have to sample the GP nodes as individual parameters instead of just constraining the statistical properties of the ensemble. This means that our model will contain of the order of $\mathcal{O}(10^2)$ parameters. This large number of parameters (and hence dimensions) renders traditional parameter space exploration techniques too slow to be feasible.

In the Metropolis-Hastings (MH) sampler [30,31], samples are drawn randomly from a proposal distribution. If the new proposal improves the fit to the data it is automatically accepted. If not, the sample has a random chance of being accepted to avoid falling into a local minimum. This means that the chance of the sampler drawing a better sample and thus of the sample being accepted decreases with the number of dimensions of the parameter space. This decreasing acceptance rate of new samples means that the time needed by samplers that randomly explore the parameter space quickly becomes unfeasible as we increase the number of parameters. This is known as the dimensionality curse.

To remedy this, in this work we make use of the No U-Turns sampler (NUTS) [32], a self-tuning version of the Hamiltonian Monte Carlo (HMC) algorithm [33,34]. HMC uses notions of Hamiltonian dynamics to draw trajectories on the parameter space along which the sampler moves. This results in a much greater acceptance rate, and allows HMC to beat the dimensionality curse. Therefore, HMC can efficiently explore parameter spaces with large numbers of dimensions in far less time than MH or nested sampling techniques [35].

The drawback of HMC is that in order to evolve the Hamiltonian equations of motion it is necessary to compute the derivatives of the likelihood with respect to the parameters. Obtaining such derivatives can be even more expensive than taking additional steps in the chains, especially in high-dimensional spaces. In order to overcome this issue, we require an inexpensive way of obtaining derivatives of the likelihood. In this work, we employ the PYTHON package PyMC3 [36] which uses the autodifferentiation [37] library Theano [38] to obtain the gradient of our model with respect to our parameters. This is achieved by drawing a symbolic graph of the model that establishes the relationship between the different variables.

Finally, our choice of NUTS over the traditional HMC is due to the fact that in the latter one needs to be able to infer *a priori* (or by trial and error) specifications such as for how long the sampler should follow the trajectory or to what precision it needs to be resolved. NUTS can tune these parameters during the burn-in phase of the chains by enforcing that the sampler does not perform a U-turn while following a trajectory, preventing the samples from becoming correlated.

III. INTERPRETING A GAUSSIAN PROCESS

In the previous section we described how to model $\mu(z)$ using a GP. In this section we discuss how to interpret it. However, as we will see, this is no easy task. The problem fundamentally stems from the fact that a GP is not a single parameter with a singular figure of merit (e.g. the standard deviation), but a vector of parameters. Nonetheless, if we wish to assess how well we can constrain $\mu(z)$ we need to devise a compact and useful way of compressing (and comparing) the information we get from the GP.

As discussed in Sec. II, the statistical properties of a GP are encapsulated in its mean and covariance matrix. Therefore, if one wishes to measure how constrained a GP is, the first intuition would be to turn to the covariance matrix of the GP's posterior—the multidimensional equivalent of the standard deviation. The problem that arises is finding a way to compress such a covariance matrix into a meaningful measurement.

A first idea would be to look at the determinant of said covariance matrix. However, the determinant mixes contributions from both the diagonal elements of the matrix (i.e. the standard deviation in each node) and the off-diagonal elements of the matrix (i.e. the correlations between the nodes) in a nontrivial way that obfuscates its interpretation. One could then think of diagonalizing the covariance matrix. However, since diagonalizing is itself a nonlinear operation interpreting the errors of the diagonal basis would be a nontrivial task.

Alternatively, one could take advantage of the so-called hyperparameters of the GP. Hyperparameters dictate the values that the nodes are allowed to take and that act as a high-level description of the statistical properties of the nodes. The most relevant hyperparameter would be the amplitude of the GP covariance matrix which dictates how much the GP can deviate from its mean. This measurement partially solves the issue of including the off-diagonal

entries in an interpretable manner since the hyperparameter controls the amplitude of both the diagonal and off-diagonal elements of the matrix. However, it is unclear how to compare two covariance matrix amplitudes with two different correlation length values. Most importantly, this measurement of uncertainty does not directly relate to the nodes of the GP themselves, only to their allowed values. In summary, there is not a singular way of quantifying the uncertainty of a GP, especially using one single number.

For the reasons discussed above in this work we use a combination of two metrics to report the constraints on the GP. At the most basic level, we study $\mu(z)$ itself and our constraints on its full redshift dependence. We pay particular attention to $\mu(z=0)$ since it gives us information on the strength of the fifth force today and can easily be related to other, laboratory or astronomical constraints [2]. On a more abstract level, we also look at the constraints on the hyperparameter η that describes the amplitude of the covariance matrix of the GP (i.e. the allowed deviation of the nodes from their mean).

IV. OBSERVABLES AND DATA SETS

As previously stated, the quality of our data is just as important as our assumptions on $H(z)$ to determine our ability to constrain $\mu(z)$. In this section, we discuss the data used in this work, as well as how we forecast what future data will be capable of.

Let us begin by discussing the currently available data. We employ the same ensemble of data used in Ref. [28], as well as additional measurements of $f\sigma_8$. These can be seen in Fig. 1 and in the summary table in the Appendix. The observables and data sets we consider are as follows.

Cosmic chronometers (CCs) are tracers of dt/dz where t is cosmic time. Since $H(z) \equiv \dot{a}/a = -(dt/dz)/(1+z)$, a measurement of dt/dz directly yields the expansion rate [39]. Here, we use the $H(z)$ measurements from CCs summarized in Table 1 of Ref. [22].

Type Ia supernovae (SNIa) are explosions of white dwarfs [40,41], which can be used as standard candles [42,43]. SNIa obey the relationship $m(z) = 5\log_{10} D_L(z) + 25 + M$, where $m(z)$ is known as the distance modulus and M is the absolute (apparent) magnitude of the SNIa. Knowing M, one can use SNIa to reconstruct $D_L(z)$. Here we use a compressed version of the Pantheon sample, known as "DS17," composed of 40 measurements of the distance modulus in the range $0.15 \leq z \leq 1.615$ [44]. We marginalize over the absolute magnitude of the supernovae as opposed to fixing its value [45]; this is equivalent to fitting the expansion rate, $E(z) = H(z)/H_0$.

Baryon acoustic oscillations (BAOs) are set by the size of the sound horizon at the end of the drag epoch ($z \sim 1020$), [46–48] $r_s(z) = \int_z^\infty [c_s/H(z')]\mathrm{d}z'$, where c_s denotes the speed of sound. The BAO feature can be measured in the directions parallel and perpendicular to the line of sight to determine $H(z)$ and $D_M(z)$ respectively. Here we use the twelfth data release of the Baryon Oscillation Spectroscopic Survey (BOSS DR12) which forms part of the Sloan Digital Sky Survey (SDSS) III. In addition to this, we employ the sixteenth data release of the extended Baryon Oscillation Spectroscopic Survey (eBOSS DR16 [49]), which forms part of the SDSS IV [50]. Finally, we make use of the *Planck* 2018 measurement of the BAO angular scale at $z_* \sim 1100$. We use the *Planck* measurement from the temperature, polarization and lensing maps combined with BAO measurements denoted as TTTEEE+LowE + Lensing + BAO.

Redshift-space distortions (RSDs) are modifications to the observed redshift of a given object caused by its radial peculiar velocity [51]. These leave a characteristic anisotropic imprint in the correlation function of galaxies that can be used to measure the growth of structure. Here, we use the three measurements of $f\sigma_8(z)$ from the BOSS DR12 data [52], and one value from the BOSS DR16 quasar sample. We include the full covariance matrix between the BAO and RSD measurements from these data sets [52,53]. We also include the $f\sigma_8$ measurements reported by the WiggleZ Dark Energy Survey [54]. Despite not being RSD based, we also include the $f\sigma_8(z=0)$ derived from the measured peculiar velocities of the Democratic Samples of Supernovae [55]. In addition

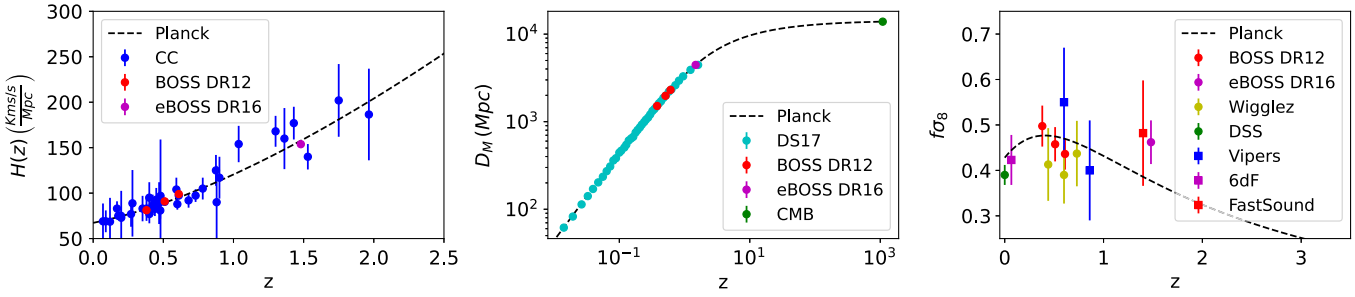

FIG. 1. Shows the data points from the different surveys used in this work across redshift for the three cosmological functions of interest $H(z)$, D_M and $f\sigma_8$.

to these, we consider three additional RSD-based $f\sigma_8$ measurements not included in Ref. [28], namely, the $f\sigma_8$ measurements from the VIMOS Public Extragalactic Redshift Survey, the 6dF Galaxy Survey and the Subaru Fibre Multi-Object Spectrograph galaxy redshift survey (FastSound).

Finally, we are interested in how future surveys will allow us to improve on current measurements. In order to do so, we generate synthetic data based on the forecast errors for the Dark Energy Spectroscopic Instrument (DESI). DESI is currently taking data from the Mayall 4 meter telescope at Kitt Peak National Observatory to construct a galaxy and quasar redshift survey. We use the forecast errors from Ref. [56] for the observables [$H(z)$, $D_A(z)$, and $f\sigma_8$] over 18 redshift bins from 0.15 to 1.85. Then, we use the fiducial values of these quantities for the best-fit *Planck* 2018 TTTEEE + LowE + Lensing + BAO ΛCDM cosmology ($\Omega_{\rm M}^{P18} = 0.315$, $\Omega_{\Lambda}^{P18} = 0.685$, $\Omega_{\rm b}^{P18} = 0.049$, $H_0^{P18} = 67.36$ and $\sigma_8^{P18} = 0.811$) to generate a synthetic data set. In the following sections, we use this synthetic data to forecast how well a stage IV survey will constrain $\mu(z)$ relative to existing data.

V. MODEL-DEPENDENT CONSTRAINTS

Having discussed our modeling of $\mu(z)$ and the data we will use to constrain it, we are now at a position to start obtaining constraints for $\mu(z)$. In this section we focus on constraints which assume a particular model for the background expansion rate $H(z)$, while modeling $\mu(z)$ as a GP. Please note that we restrict ourselves to models without curvature (i.e. $\Omega_k = 0$). This is motivated by the results of Baker *et al.* [7] where it was shown that the equation of state for the energy component responsible for the accelerated expansion of the Universe would be degenerate with $\mu(z)$.

We start by considering a fiducial expansion rate, i.e., the expansion rate given by the *Planck* 2018 [9] ΛCDM TTTEEE + LowE + Lensing + BAO posteriors. In this setup, we only make use of our $f\sigma_8$ measurements to constrain our model since we are already using *Planck* 2018's posterior as a constraint on the expansion history. The parameters varied in this setup with their respective priors can be found in the first column of Table III. This will give us a best-case scenario and will allow us to identify a benchmark against which all other constraints can be compared.

We then relax this assumption, removing the *Planck* prior and freeing up the ΛCDM parameters where,

$$H(z) = H_0\sqrt{\Omega_M(1+z)^3 + \Omega_R(1+z)^4 + \Omega_\Lambda}, \quad (7)$$

and Ω_M, Ω_R and Ω_Λ are the cosmological matter, radiation and dark energy densities, respectively, today. We then use the measurements of $H(z)$, $D_M(z)$ and $f\sigma_8$ to constrain these parameters at the same time that we constrain $\mu(z)$. The details of this model can be found in the second column of Table III.

In the next study case, to further loosen our assumptions, we chose a background rate of expansion using a general model of dark energy with an equation of state $w(a) = w_0 + w_a(1-a)$ (wCDM). In such a model the expression for the expansion rate becomes

$$H(z) = H_0\sqrt{\Omega_M(1+z)^3 + \Omega_R(1+z)^4 + \Omega_\Lambda(1+z)^{\nu(z)}}, \quad (8)$$

where

$$\nu(z) = \frac{3(1 + w_0 + z(1 + w_0 + w_a))}{1+z}. \quad (9)$$

Similarly to ΛCDM, we consider two cases. In the first case, we use a fiducial wCDM expansion rate given by *Planck*'s wCDM TTTEEE + lowE + lensing + BAO + SNe posteriors, where we only use $f\sigma_8$ measurements to constrain our model. We include SNIa measurements since the TTTEEE + lowE + lensing + BAO combination considered so far is not able to place tight constraints on the equation of state on its own. The details for this model can be found in the third column of Table III. In the second case, we free the expansion rate parameters (including w_0 and w_a) and use our whole suite of measurements to inform our constraints. The details of this model can found in the fourth column of Table III.

We find that regardless of the model assumptions made (ΛCDM or wCDM), $\mu(z)$ is in excellent statistical agreement with the GR value $\mu(z) = 1$ at all redshifts up to 1σ. We find the same consistency with GR when using the *Planck* 2018 prior on the cosmological parameters (including w_0 and w_a in the wCDM case) and when freeing them. Figure 2 shows the constraints obtained on $\mu(z)$ in both cases, with the constraints obtained assuming ΛCDM shown in the top panel and those assuming wCDM in the bottom panel. In both panels we compare the contours obtained using the *Planck* 2018 posterior as a prior in combination with our $f\sigma_8$ measurements, and by using our whole suite of measurements to inform our constraints. We can see that imposing the *Planck* 2018 prior significantly reduces the uncertainty on $\mu(z)$ at all redshifts. More quantitatively (see Table I), the uncertainty on μ_0 decreases by roughly ∼35% for either a ΛCDM or wCDM cosmology and, remarkably, the uncertainty in μ_0 remains unchanged when using the more complex wCDM background model. Thus, we can conclude that the combination of cosmic chronometer, BAO and SNIa data are sufficiently precise to pin down the equation of state for the purpose of constraining μ_0.

It is interesting to understand this result in light of the discussion in Ref. [7]. There, it was shown that, while a measurement of $f\sigma_8$ at one redshift would lead to a severe

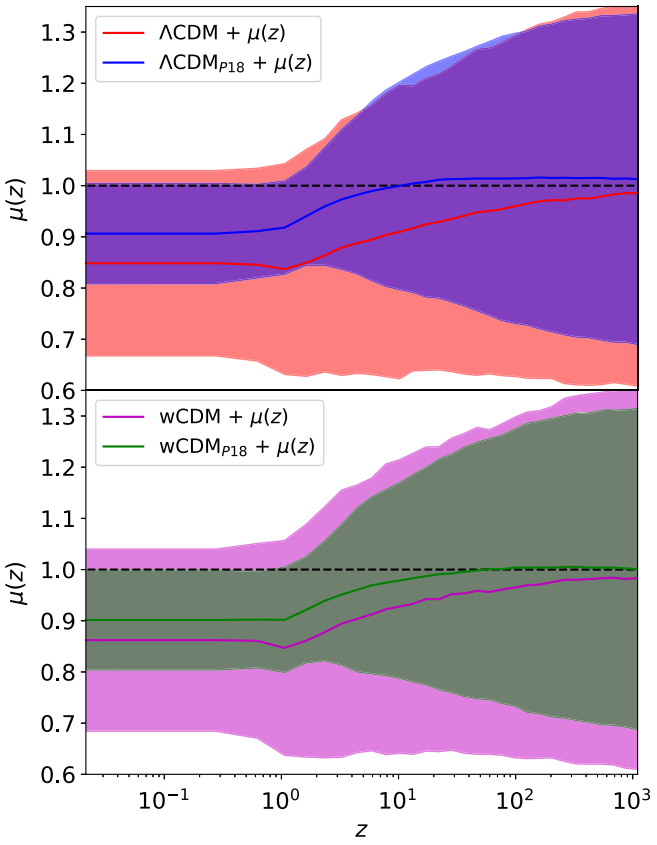

FIG. 2. Obtained model-dependent constraints on $\mu(z)$. Top: constraints obtained assuming a ΛCDM model for $H(z)$ both when when using *Planck* 2018's ΛCDM posterior as a prior and when using current late-time data to inform it (blue and red respectively). Bottom: equivalent wCDM constraints (green and purple respectively).

degeneracy between μ and w, measurements at multiple redshifts combined with distance measurements could, in principle, break this degeneracy and decorrelate constraints between the two parameters. In Fig. 3 we see this idea in action. In this figure we show the 1D and 2D distributions for the parameters w_0, w_a and μ_0. We superpose the contours obtained when using the *Planck* 2018 prior (blue) and when only using current data to constrain the wCDM parameters (red). As we can observe, the current data contours show a degeneracy between w_0 and w_a which is not present when using the *Planck* 2018 prior. However, neither w_0 nor w_a are degenerate with μ_0 in any case.

We further note that the uncertainty in $\mu(z)$ increases as we look at higher redshifts but not excessively so. Two factors are at play here. First, since the data are nonlocal functions of $\mu(z)$ [i.e. $\mu(z)$ needs to be integrated to solve for f in Eq. (3)], they allow us to place constraints on higher redshift values of $\mu(z)$. In addition to this, we are marginalizing over the hyperparameters of the Gaussian process. This means that the data at lower redshifts can put a constraint on the amplitude and correlation length of the GP's kernel. This effectively limits the variance of the GP even in regions with no data.

We have seen that assuming a wCDM for $H(z)$ as opposed to a ΛCDM model does not degrade our constraints on $\mu(z)$. It is then interesting to explore the relationship between $\mu(z)$ and other cosmological parameters of our models, particularly Ω_M and σ_8. Figure 4 shows the 1D and 2D contours for the parameters Ω_M, σ_8 and μ_0 obtained when assuming the ΛCDM and wCDM models to parametrize $H(z)$. In each panel we superpose the results obtained when assuming *Planck* 2018's posterior as a prior for the expansion rate as opposed to letting background data inform the constraints. We show the associated numerical constraints in Table I. We also display the constraints obtained by fitting a ΛCDM model and a wCDM model while keeping $\mu(z) = 1$ (i.e. GR) for context.

Looking at Eq. (3) one would expect a great degeneracy between Ω_M and $\mu(z)$. However, if we look at the bottom left corner panel (ΛCDM) and top right panel (wCDM) of Fig. 4 we can see how information about the background breaks this degeneracy. Therefore, it is not clear that a better constraint on one will lead to an improvement in the other.

We show our constraints on Ω_M for the different models in Fig. 5, including constraints for the ΛCDM and wCDM models when keeping $\mu(z) = 1$ (i.e. GR) for reference. Regardless of whether we assume a ΛCDM or wCDM model for $H(z)$ we obtain a slightly lower value for Ω_M than the one obtained by *Planck* 2018 (and the one obtained using *Planck* 2018's posterior as a prior). Nonetheless, once the size of the error bars is taken into account, the constraints are in reasonable statistical agreement (less than 1.5σ tension). Moreover, assuming wCDM systematically results in a lower yet statistically compatible constraint of

TABLE I. Model-dependent constraints on Ω_M, σ_8 and μ_0, including mean values and 1σ errors.

	Ω_M	σ_8	μ_0
ΛCDM	0.302 ± 0.007	0.789 ± 0.027	⋯
wCDM	0.292 ± 0.013	0.801 ± 0.034	⋯
$\mu(z) + \Lambda\text{CDM}_{P18}$	0.314 ± 0.007	0.811 ± 0.006	0.904 ± 0.123
$\mu(z) + w\text{CDM}_{P18}$	0.306 ± 0.008	0.821 ± 0.014	0.899 ± 0.123
$\mu(z) + \Lambda\text{CDM}$	0.302 ± 0.007	0.878 ± 0.127	0.850 ± 0.191
$\mu(z) + w\text{CDM}$	0.29 ± 0.016	0.887 ± 0.127	0.862 ± 0.190

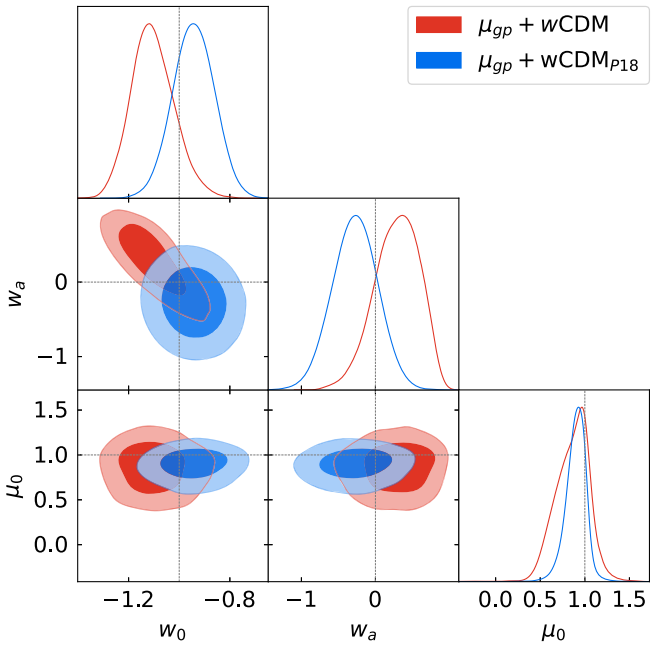

FIG. 3. Constraints for the cosmological parameters w_0, w_a and μ_0. Diagonal panels show 1D distributions. Off-diagonal panels show 2D distributions. In each panel we superpose the contours obtained when assuming *Planck* 2018's wCDM posterior as a prior (blue) and when marginalizing over a wCDM background (red) given current late-time data.

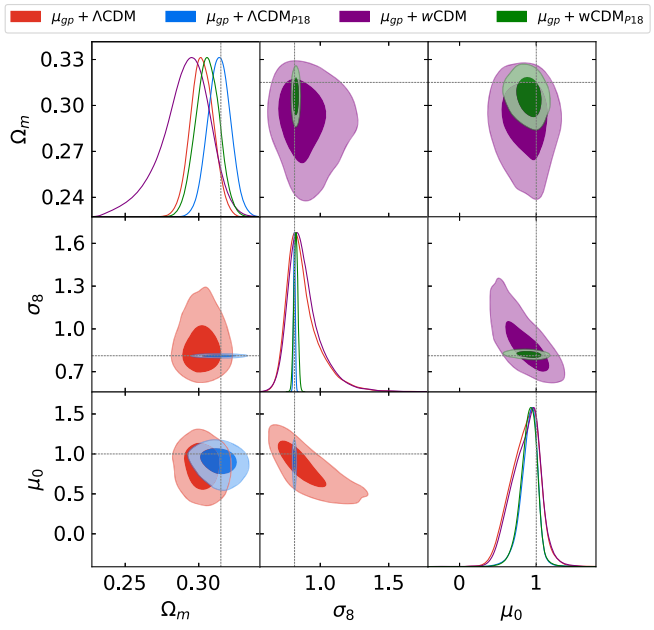

FIG. 4. Constraints for the cosmological parameters Ω_M, σ_8 and μ_0. Diagonal panels show 1D distributions. Off-diagonal panels show 2D distributions. The bottom triangle shows the constraints obtained when assuming a ΛCDM background both when imposing *Planck* 2018's ΛCDM posterior as a prior (blue) and when using current late-time data to inform it (red). The top triangle shows the equivalent constraints when a wCDM background is assumed instead (green and purple respectively).

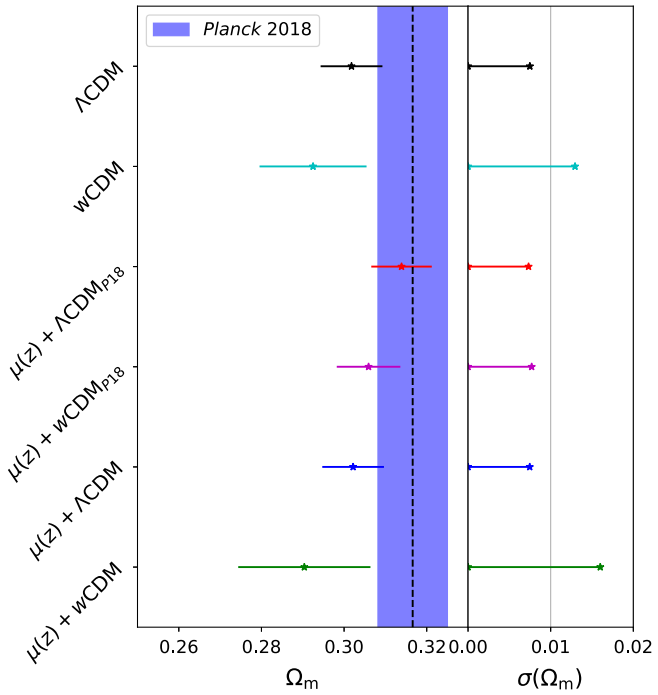

FIG. 5. Constraints obtained for Ω_M for each model considered in this work. The side panel shows the uncertainty of each constraint.

Ω_M than assuming a ΛCDM model. Finally, it is interesting to note that introducing $\mu(z)$ barely degrades the constraint on Ω_M if the background is ΛCDM. On the contrary, for a wCDM model, introducing $\mu(z)$ leads to a ∼20% larger error bar on Ω_M. This is caused by the fact that freeing the equation of state reduces the ability of the background to constrain Ω_M and, thus, the wCDM Ω_M constraint increasingly depends on the growth data to inform its value.

Moving to σ_8, current growth data cannot break the degeneracy between σ_8 and μ_0. This can be seen in the middle panel of the bottom row and the right panel of the middle row. Therefore, when assuming a model for $H(z)$, the bottleneck in constraining μ_0 is how well we know σ_8. This explains why our constraints on $\mu(z)$ drastically improve when imposing the *Planck* 2018 prior since it imposes a much tighter constraint on σ_8, breaking the degeneracy with $\mu(z)$.

VI. MODEL-INDEPENDENT CONSTRAINTS

We now proceed to further relax our assumptions about the background expansion rate by promoting $H(z)$ to a GP. We do so by following the methodology developed in Ref. [28]. More specifically, we model $H(z)$ as

$$H(z) = A_0 H^{P18}(z)(1 + \delta H_{gp}), \tag{10}$$

where A_0 is a free parameter, $H^{P18}(z)$ is the Hubble rate for our ΛCDM *Planck* 2018 best-fit fiducial cosmology

(see Sec. II), and δH_{gp} is a relative deviation that we model as a Gaussian process. This is a Bayesian approach to GPs in which one marginalizes simultaneously over the GP itself and its mean. In Ref. [28] we showed that this approach shields our cosmological constraints from potential biases introduced by our choice of mean function. More recently, Hwang *et al.* [57] showed that unphysical oscillations can appear in the reconstructed functions if one does not marginalize over a possible family of mean functions for the GP. However, it is worth noting that the degeneracies between the GP and the $A0$ parameter make exploring the parameter space significantly more expensive.

Therefore, our inference process now involves two GPs. This allows us to measure the degeneracy between modifications of the expansion history and the Poisson equation in the prediction of $f\sigma_8$ without having to assume a particular model.

However, becoming fully model independent comes at the cost of no longer being able to constrain Ω_M with measurements of background quantities. This is because $H(z)$ is no longer a function of cosmological parameters. Thus, we have no independent way of constraining Ω_M apart from the relationship between $H(z)$ and $f\sigma_8(z)$. Revisiting Eq. (3), we can also see that we are now faced with an unbreakable degeneracy between Ω_M and $\mu(z)$. In order to deal with this degeneracy, in this section we consider the new, combined parameter

$$\tilde{\mu}(z) = \frac{\Omega_M}{\Omega_M^{P18}}\mu(z), \tag{11}$$

where Ω_M^{P18} is the *Planck* 2018 TTTEEE + LowE + Lensing + BAO, ΛCDM best-fit value of Ω_M.

In order to solve Eqs. (3) and (6) when considering two GPs, we employ the same combination of numerical methods as in Ref. [28] [where we also modeled $H(z)$ as a GP], albeit with some modification. In Ref. [28] we assigned a node of the GP to each node of the numerical grid used to solve the growth equation and the comoving distance integral. This approach becomes very computationally expensive when we introduce a second GP. In order to make our model more computationally efficient, we decouple the number of nodes in the numerical integration schemes from the number of nodes used for each GP, linearly interpolating where necessary. This allows us to significantly reduce the number of parameters of the model while preserving the necessary numerical accuracy. Reducing the number of nodes in the GPs means that the degeneracy between the remaining nodes is reduced. This latter aspect is particularly helpful when using the HMC algorithm which is most efficient when the parameters are as uncorrelated as possible. The end result of reducing the number of parameters and the degeneracy between them is a substantial speedup in the time needed for the sampler to converge.

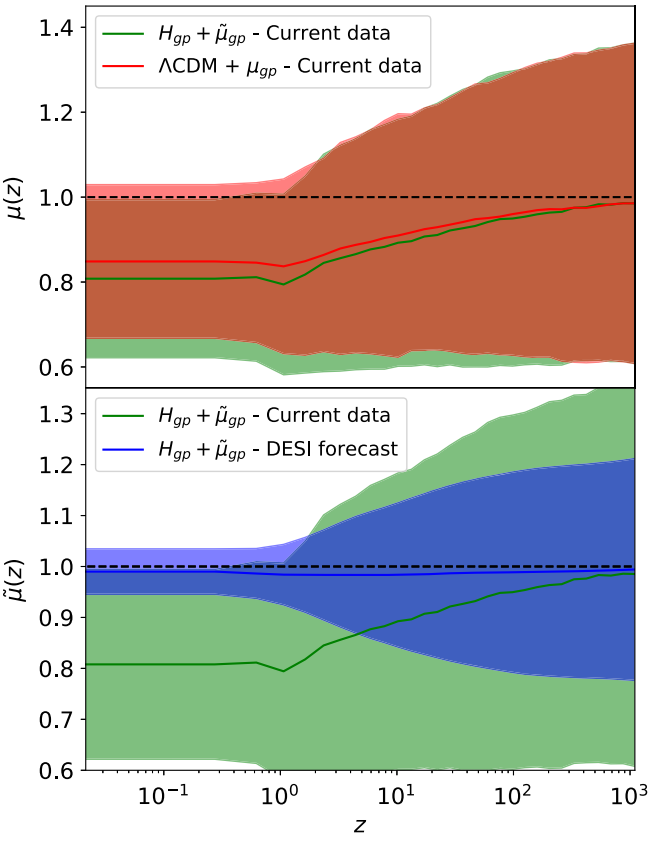

FIG. 6. Top: constraints on $\mu(z)$ for current data when assuming the ΛCDM model to model the background expansion of the Universe (red) and when using a second GP (green). Note that when using a second GP the quantity being constrained is $\tilde{\mu}(z)$ as opposed to $\mu(z)$. Bottom: constraints obtained on $\tilde{\mu}(z)$ when using a second GP to model $H(z)$ for both current data (green) and mock DESI data (blue).

We show the obtained model-independent constraints for $\tilde{\mu}(z)$ in Fig. 6. On the one hand, in the top panel of the figure, we can observe that the model-independent constraints on $\tilde{\mu}(z)$ are only marginally worse than the model-dependent constraints on $\mu(z)$ (5–10% depending on whether we consider the ΛCDM or wCDM model). This means that, even when completely relaxing our assumptions about $H(z)$, current data have enough constraining power to break the degeneracy between $H(z)$ and $\tilde{\mu}(z)$. This can be further seen in the correlation matrix between the GP's nodes of $\tilde{\mu}(z)$ and $H(z)$. Figure 7 shows that, although $\mu(z)$ and $H(z)$ nodes have a great degree of autocorrelation (as expected for a GP), the correlation coefficients between both quantities are never larger than 5%. This can be seen as a generalization of the lack of correlation we observed between the background parameters and μ_0 in Sec. V. Moreover, we can see that $H(z)$'s low-redshift nodes are much less correlated with high-redshift nodes than those of $\widetilde{\mu(z)}$.

It is important to bear in mind that these are constraints on $\tilde{\mu}(z)$, not on $\mu(z)$. Converting constraints on $\tilde{\mu}(z)$ into

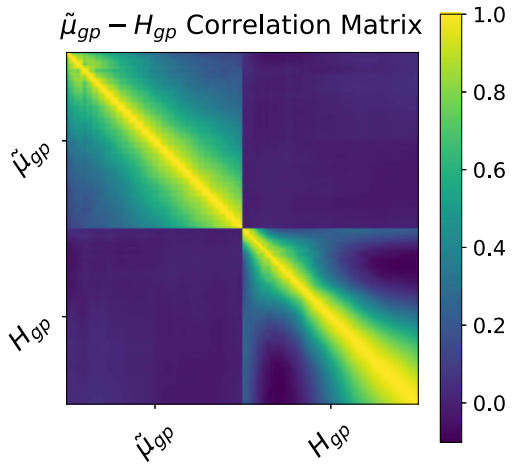

FIG. 7. Correlation coefficients between the nodes of the GP on $H(z)$ and the GP on $\mu(z)$. This plot can be seen as a generalization of Fig. 3. Note, that current data is powerful enough to constrain the expansion rate and the modifications of the linear growth independently as shown by the lack of correlations between the two quantities.

constraints on $\mu(z)$ requires a measurement of Ω_M. However, in the process of freeing $H(z)$ we have lost all of our knowledge of Ω_M. Thus, an external, model-independent measurement of Ω_M would be needed to transform $\tilde{\mu}(z)$ constraints into $\mu(z)$ constraints. The constraints on $\tilde{\mu}(z)$ should therefore be understood as the most optimistic model-independent constraint on $\mu(z)$ possible given current data, i.e. the case for which we have a perfect model-independent measurement of Ω_M.

Finally, we find $\sigma_8 = 0.886 \pm 0.138$ when a second GP is used to model $H(z)$. This means that not assuming a ΛCDM or wCDM model for the expansion history degrades our σ_8 constraint by around ∼10%. Nonetheless, the degree of correlation between σ_8 and $\tilde{\mu}_0$ remains virtually identical to that of model-dependent analyses. Thus, model-independent constraints on $\tilde{\mu}(z)$ will also benefit greatly from ways of tightening their constraint on σ_8, just as we saw in the model-dependent case. We will discuss this further in the next section when considering our analysis of mock DESI data.

VII. DISCUSSION

In this paper we have assessed the effect of our current knowledge of the expansion rate history on our ability to constrain $\mu(z)$ in a model-independent manner. As was argued in Refs. [7,8], the assumptions that go into modeling the Hubble rate as a function of redshift, $H(z)$ will impact constraints on $\mu(z)$ from the growth rate of structure. It was shown that the more conservative (or looser) the model for $H(z)$, the weaker the constraints on $\mu(z)$ should be.

We have found that, however, current constraints on the expansion rate from cosmic chronometer, supernova and BAO data are sufficiently tight that the assumptions made about the underlying background model are not important when constraining $\mu(z)$. To show this, we have used a completely general form for $\mu(z)$ (a Gaussian process), and quantified whether assuming a simple equation of state for dark energy ($w = -1$), or a more general equation of state of the form $w = w_0 + w_a(1-a)$ affects the final constraints on $\mu(z)$. We also considered a completely general form for $H(z)$ which we also modeled as a Gaussian process. In this case, we are faced with a fundamental degeneracy between $\mu(z)$ and Ω_M and thus, we present our results in terms of $\tilde{\mu}(z) = \Omega_M \mu(z)/\Omega_M^{P18}$ where we recall that Ω_M^{P18} is the best-fit value of Ω_M for the *Planck* 2018 TTTEEE + LowE + Lensing + BAO analysis of the ΛCDM model.

As discussed in Sec. III, we summarize our results on the constraints on $\mu(z)$ using two statistics. On the one hand, we look at the uncertainty in $\mu_0 \equiv \mu(z=0)$ as it directly relates to the strength of any possible fifth force today. On the other hand, we consider the mean value of the amplitude of the Gaussian process covariance matrix, η_μ, which is an abstract measurement of the uncertainty of the Gaussian process through its whole domain.

We present the corresponding results in Fig. 8. Reassuringly, we find that the two statistics offer us the same picture: the less assumptions we make about the expansion history, the more uncertainty there is in $\mu(z)$. However, it is extremely important to stress that the loss in constraining power is marginal. Comparing assuming a ΛCDM vs wCDM model, we find that it makes effectively no difference and there is no degradation in our constraints on $\mu(z)$. Even when a second GP is used to model $H(z)$ the constraint is only a few percent larger.

Focusing on μ_0, we find that $\sigma(\mu_0) \simeq 0.12$ if we assume *Planck* 2018's posterior as a prior, for either the ΛCDM or wCDM model. This uncertainty increases to $\sigma(\mu_0) \simeq 0.19$ if instead of imposing *Planck* 2018's posterior as a prior we use our collection of late-time $H(z)$, $D_M(z)$ and $f\sigma_8$ measurements to inform our constraints. The main difference between assuming *Planck* 2018 posteriors and using late-time data to inform our models is that the former provides us with a much tighter constraint on σ_8, the main bottleneck when constraining $\mu(z)$ in a model-dependent fashion. Looking at the model-independent constraint, we find that $\sigma(\tilde{\mu}(z)) \simeq 0.21$.

If we instead look at the constraints on η_μ, we find the exact same trend as in μ_0. While one would expect the two statistics to agree, μ_0 only probes the GP at $z = 0$ while η_μ contains information about the whole GP domain. We find that for our best-case scenario, in which we assume *Planck* 2018's ΛCDM background, $\eta_\mu = 0.25$. Letting late-time data inform a ΛCDM model instead returns $\eta_\mu = 0.32$. Furthermore, if we assume a wCDM model, we find $\eta_\mu = 0.26$ when using *Planck*'s posteriors to pin it and $\eta_\mu = 0.32$ when letting late-time data inform it. Finally, we find $\eta_\mu = 0.33$ in the model-independent case.

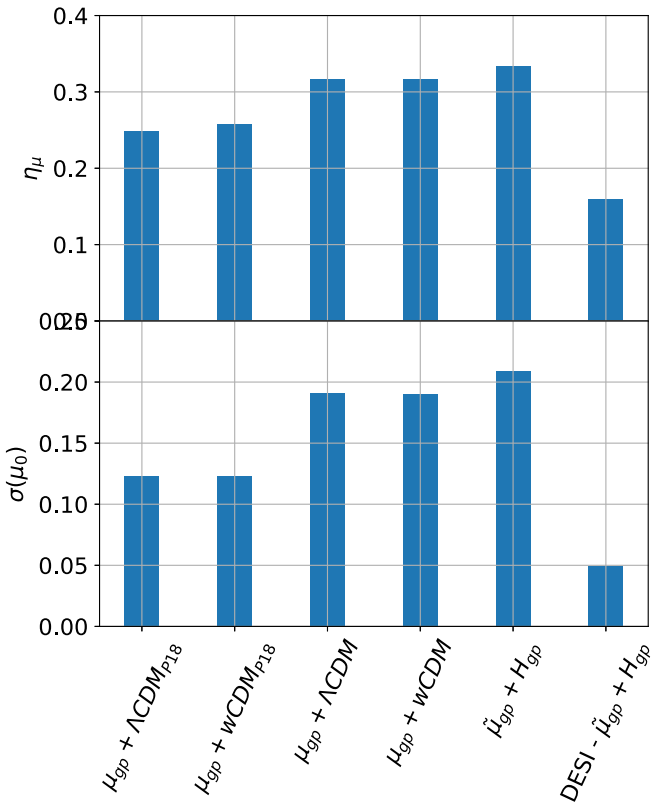

FIG. 8. Comparison of different measures of uncertainty in $\mu(z)$ between the different models considered in this work. The top panel shows the mean value of the amplitude of the covariance matrix of $\mu(z)$ for each model. The bottom panel shows the uncertainty in $\mu(z=0) \equiv \mu_0$. Note that when a second GP is considered to model $H(z)$ (i.e. last two entries) $\tilde{\mu}(z)$ is shown as opposed to $\mu(z)$.

The fact that constraints on μ are (relatively) insensitive to our parametrization of $H(z)$ is not unexpected. This is because current background data is powerful enough to constrain $H(z)$ independently of the assumptions made. In the analysis of Ref. [28], we found that constraints on Ω_M from the growth rate were not strongly dependent on our modeling choices of the Gaussian process on $H(z)$.

There have been other attempts at constraining $\mu(z)$. In Ref. [9] an uncertainty of $\sigma(\mu_0) \simeq 0.25$ was found under the assumption that μ evolves as $\mu(z) - 1 \propto [1 - \Omega_M(z)]$. However, different assumptions about the specific time dependence of μ [e.g. $\mu(z) \propto a^n$] lead to constraints that are strongly dependent on the choice of n [11], with μ_0 in the range $\sigma(\mu_0) \in (0.04, 1.5)$. Assuming that the modified Poisson equations arise from scalar-tensor theories, one can use the tools of effective field theory [15] or simply assume specific classes of models [14] to obtain $\sigma(\mu_0) \simeq 0.25$. As we can see, our methodology returns stronger constraints with $\sigma(\mu_0) \in (0.12, 0.19)$ depending on the strength of the assumptions made on $H(z)$. We note however that it can be misleading to directly compare $\sigma(\mu_0)$ as it can be heavily dependent on the underlying model and choice of data sets one is using.

It is instructive to see how much our constraints will improve with future data. As an example, we choose the specifications for the DESI data set, described in Sec. IV, and combine it with the *Planck* 2018 cosmic microwave background (CMB) BAO measurement to pin down the GP on $H(z)$ at high redshift. Our analysis of DESI mock data shows that we will obtain constraints on $\tilde{\mu}(z)$ [i.e. with a model-independent $H(z)$] which are twice as tight as with current data when assuming either a ΛCDM or wCDM background. This is in spite of the DESI constraint on σ_8 being about 6 times wider than *Planck* 2018's. The reason behind this improvement in constraining power boils down to the fact that DESI alone will offer nearly twice as many measurements on $f\sigma_8$ as the number considered in this work over a larger redshift window. Moreover, DESI $f\sigma_8$ measurements will have significantly smaller error bars than currently available ones. It is particularly important to focus on the smaller size of said error bars relative to the expected dynamic range of $f\sigma_8$ in the redshift window probed. This will greatly help break the degeneracy between the amplitude of $f\sigma_8$ (given by σ_8) and its shape [given by $\mu(z)$ in the presence of background data to pin down Ω_M] present in current data.

Finally, there are several avenues through which the results and methodology presented here could be further explored. One can ask the question: how well do we need to measure Ω_M to obtain a competitive model-independent constraint on $\mu(z)$ with current data? Using propagation of errors, $\sigma(\mu)/\mu = \sqrt{(\sigma(\tilde{\mu})/\tilde{\mu})^2 + (\sigma(\Omega_M)/\Omega_M)^2}$, we find that model-independent measurements of Ω_M to 10% precision would be enough to match model-independent constraints on $\mu(z)$ to model-dependent constraints with current data. Similarly, a percentage model-independent measurement of Ω_M would allow us to constrain $\mu(z)$ to virtually the same precision as $\tilde{\mu}(z)$. This measurement of Ω_M would need to be independent from the model assumed for the background expansion and for the parametrization of the Poisson equation. Future works could attempt to obtain an alternative model-independent constraint on Ω_M to break the $\tilde{\mu}(z) - \Omega_M$ degeneracy found in this methodology.

ACKNOWLEDGMENTS

All authors contributed to the development and writing of this paper. We would like to thank Dan Foreman-Mackey and Andreu Font-Ribera for their helpful comments. We acknowledge support from the Beecroft Trust. C. G.-G. and P. G. F. acknowledge funding from the European Research Council under the European Unions Horizon 2020 research and innovation programme (grant agreement No 693024). DA acknowledges support from the Science and Technology Facilities Council through an Ernest Rutherford Fellowship, grant reference ST/P004474. J. R.-Z. is supported by an

STFC doctoral studentship. The analysis made use of the software tools PyMC3 [36], THEANO [38], NumPy [58], MATPLOTLIB [59], CLASS [60], and GetDist [61].

APPENDIX: TABLES

In this appendix we display the large tables that would have interrupted the reading flow of the main text of the paper. Table II contains the data sets used in this work.

Table III contains the prior distributions assumed for each of our models. In general, the priors are chosen broad enough to prevent them from biasing our results. In particular, the priors on the hyperparameters of the GP on $\mu(z)$ ($\eta_\mu l_\mu$), are common to all of the studied cases. As discussed in Ref. [28], when using gradient-based methods it is best practice to use smooth priors unless there is a physical limit on the values that the parameter can take (e.g. $\Omega_M \in [0,1]$).

Thus, the prior of the amplitude of the GP, η_μ, is a half-normal distribution $\mathcal{N}_{1/2}(0,0.5)$, i.e. centered at 0 with 0.5 standard deviation. On the other hand, the correlation length l_μ has an uniform prior $U(0.01,6)$. The reason for a uniform prior (i.e. not smooth) is twofold. On the one hand, when sampling l_μ it is extremely important to avoid small values in order to avoid volume effects [see Eq. (5)]. On the other hand, we do not want to down-/up-weight a particular correlation scale for the nodes of the GP.

Moving on to the cosmological parameters, only Ω_M has a uniform prior $U(0,1)$ to enforce the physical limits on the values of the parameter. All the others have normal distributions whose details can be found in Table III. For the cases with a *Planck* 2018 prior, we use the values quoted in Ref. [9]. In particular, for the $\Lambda\text{CDM}_{P18}+\mu_{\text{GP}}$ case (second column), we use the TTTEEE + lowE + lensing + BAO ΛCDM constraints (last column of Table 2 in Ref. [9]), while for the $w\text{CDM}_{P18}+\mu_{\text{GP}}$ case (fourth column), we use the TTTEEE + lowE + lensing + BAO + SNe wCDM constraints (first column of Table 6 in Ref. [9]). Note that in the wCDM case the constraints also include SNIa data which is not present in the ΛCDM constraints. This is because TTTEEE + lowE + lensing + BAO data cannot constrain wCDM models by itself. Note that for both the ΛCDM and wCDM models we fix $\Omega_R = 9.245\times10^{-5}$. Ω_Λ is then derived using $1=\Omega_M+\Omega_R+\Omega_\Lambda$.

We must also consider a number of nuisance parameters needed to model the specific data sets chosen for this work. For instance, in order to relate the luminosity curves of the Pantheon data set to luminosity distances one needs to know the value of the absolute magnitude of the supernovae, M. In this work we choose the agnostic way and marginalize over M, assuming a normal prior $\mathcal{N}(-19.2,1)$, which encompasses the H_0 values of both Riess *et al.* [68] and the Planck Collaboration *et al.* [9]. On the other hand, we make extensive use of measurements of both parallel and perpendicular BAO measurements. In order to relate these measurements to $H(z)$ and $D_M(z)$ one needs to know the value of the sound horizon at either drag (r_d) or recombination (r^*) epochs. In order to obtain r_d and r^* we use a modified version of the Eisenstein-Hu fitting formula [69,70] given by

$$r_d \approx \frac{45.5337\ln(7.20376/\omega_m)}{\sqrt{1+9.98592\omega_b^{0.801347}}}\text{Mpc}, \tag{A1}$$

where $\omega_m=\Omega_M(H_0/100)^2$ and $\omega_b=\Omega_b(H_0/100)^2$. Then, noting that the ratio between r_d and r^* can be approximated as a function exclusively of Ω_b, we derive the fitting formula

$$\left(\frac{r_d}{r^*}\right)(\Omega_b) \approx 1.11346 - 2.7985\Omega_b + 16.5111\Omega_b^2. \tag{A2}$$

Hence, by combining Eqs. (A1) and (A2) we can obtain a prediction for $r^\star$. This approach is capable of reproducing the CLASS ΛCDM predictions for r_d and r^* to an average

TABLE II. Data sets used in our analysis, listing the probe, the redshift range of the probe, the choice of observable and the size of the data vector.

Data set	Probe	Redshifts	Observable			Data points
			$H(z)$	$D_m(z)$	$f\sigma_8$	
CCs [22]	Cosmic chronometers	0.07–1.965	✓	×	×	33
Pantheon DS17 [44]	SNIa	0.38–0.61	×	✓	×	40
BOSS DR12 [52]	BAO + RSD	0.38–0.61	✓	✓	✓	3 × 3
eBOSS DR16 [62]	BAO + RSD	1.48	✓	✓	✓	1 × 3
WiggleZ [63]	RSD	0.44–0.73	×	×	✓	3
Vipers [64]	RSD	0.60–0.86	×	×	✓	2
6dF [65]	RSD	0.067	×	×	✓	1
FastSound [66]	RSD	1.4	×	×	✓	1
DSS [67]	RSD	0	×	×	✓	1
Planck 2018 [9]	CMB	1090.30	×	✓	×	1
DESI [56]	BAO + RSD	0.15–1.85	✓	✓	✓	3 × 18

TABLE III. Priors used for the different parameters of the models considered in this work. The first column shows the complete list of parameters. U stands for a uniform distribution; $\mathcal{N}(a,b)$ and $\mathcal{N}_{1/2}(a,b)$, for a normal and half-normal distribution, respectively, centered at a and with standard deviation b. Empty entries represent parameters not sampled by the model.

	$H_{\Lambda\mathrm{CDM},P18}+\mu_{gp}$	$H_{\Lambda\mathrm{CDM}}+\mu_{gp}$	$H_{w\mathrm{CDM},P18}+\mu_{gp}$	$H_{w\mathrm{CDM}}+\mu_{gp}$	$H_{gp}+\tilde{\mu}_{gp}$
A_0	⋯	⋯	⋯	⋯	$\mathcal{N}(1.0,0.2)$
η_{H}	⋯	⋯	⋯	⋯	$\mathcal{N}_{1/2}(0,0.2)$
l_{H}	⋯	⋯	⋯	⋯	$U(0.01,6)$
η_{μ}	$\mathcal{N}_{1/2}(0,0.5)$	$\mathcal{N}_{1/2}(0,0.5)$	$\mathcal{N}_{1/2}(0,0.5)$	$\mathcal{N}_{1/2}(0,0.5)$	$\mathcal{N}_{1/2}(0,0.5)$
l_{μ}	$U(0.01,6)$	$U(0.01,6)$	$U(0.01,6)$	$U(0.01,6)$	$U(0.01,6)$
Ω_{m}	$\mathcal{N}(0.316,0.008)$	$U(0,1)$	$\mathcal{N}(0.307,0.011)$	$U(0,1)$	⋯
Ω_{b}	⋯	$U(0.03,0.07)$	⋯	$U(0.03,0.07)$	$U(0.03,0.07)$
H_0	$\mathcal{N}(67.27,0.6)$	$\mathcal{N}(70,5)$	$\mathcal{N}(68.31,0.82)$	$\mathcal{N}(70,5)$	⋯
σ_8	$\mathcal{N}(0.811,0.007)$	$\mathcal{N}(0.8,0.5)$	$\mathcal{N}(0.82,0.011)$	$\mathcal{N}(0.8,0.5)$	$\mathcal{N}(0.8,0.5)$
w_0	⋯	⋯	$\mathcal{N}(-1,0.5)$	$\mathcal{N}(-0.957,0.08)$	⋯
w_a	⋯	⋯	$\mathcal{N}(0,0.5)$	$\mathcal{N}(-0.29,0.3)$	⋯
M	⋯	$\mathcal{N}(-19.2,1)$	⋯	$\mathcal{N}(-19.2,1)$	$\mathcal{N}(-19.2,1)$
r_d	⋯	Derived	⋯	Derived	$\mathcal{N}(150,5)$
r^*	⋯	Derived	⋯	Derived	Derived

of 1.5% precision within the considered $\Omega_M \in [0.1, 0.6]$ and $\Omega_b \in [0.03, 0.07]$. Since the wCDM model we consider does not include early dark energy, we can also use Eqs. (A1) and (A2) to predict the values of r_d and r^* in such case. On the other hand, when a second GP is used to model $H(z)$, Ω_M is absorbed into the GP on $\mu(z)$ to form $\tilde{\mu}(z)$. This disallows us from following the same approach to obtain r_d and r^* as when assuming a ΛCDM or wCDM model. In this scenario we sample r_d directly as a parameter from $\mathcal{N}(145,5)$. Then, to get r^* we use Eq. (A2) as a function of r_d and Ω_b using the same Ω_b as in the ΛCDM and wCDM case.

[1] P. G. Ferreira and C. Skordis, The linear growth rate of structure in parametrized post Friedmannian Universes, Phys. Rev. D **81**, 104020 (2010).

[2] P. G. Ferreira, Cosmological tests of gravity, Annu. Rev. Astron. Astrophys. **57**, 335 (2019).

[3] E. G. Adelberger, B. R. Heckel, and A. E. Nelson, Tests of the gravitational inverse square law, Annu. Rev. Nucl. Part. Sci. **53**, 77 (2003).

[4] T. Clifton, P. G. Ferreira, A. Padilla, and C. Skordis, Modified gravity and cosmology, Phys. Rep. **513**, 1 (2012).

[5] A. Joyce, B. Jain, J. Khoury, and M. Trodden, Beyond the cosmological standard model, Phys. Rep. **568**, 1 (2015).

[6] P. J. E. Peebles, *The Large-Scale Structure of the Universe* (Princeton University Press, 1980), ISBN: 978-0-691-08240-0.

[7] T. Baker, P. Ferreira, and C. Skordis, A fast route to modified gravitational growth, Phys. Rev. D **89**, 024026 (2014).

[8] F. Simpson and J. A. Peacock, Difficulties distinguishing dark energy from modified gravity via redshift distortions, Phys. Rev. D **81**, 043512 (2010).

[9] N. Aghanim *et al.*, Planck 2018 results. VI. Cosmological parameters, Astron. Astrophys. **641**, A6 (2020).

[10] S. Joudaki *et al.*, KiDS-450 + 2dFLenS: Cosmological parameter constraints from weak gravitational lensing tomography and overlapping redshift-space galaxy clustering, Mon. Not. R. Astron. Soc. **474**, 4894 (2018).

[11] E.-M. Mueller, W. Percival, E. Linder, S. Alam, G.-B. Zhao, A. G. Sánchez, F. Beutler, and J. Brinkmann, The clustering of galaxies in the completed SDSS-III Baryon Oscillation Spectroscopic Survey: Constraining modified gravity, Mon. Not. R. Astron. Soc. **475**, 2122 (2018).

[12] J. Espejo, S. Peirone, M. Raveri, K. Koyama, L. Pogosian, and A. Silvestri, Phenomenology of large scale structure in scalar-tensor theories: Joint prior covariance of w_{DE}, Σ and μ in Horndeski, Phys. Rev. D **99**, 023512 (2019).

[13] L. Pèrenon, F. Piazza, C. Marinoni, and L. Hui, Phenomenology of dark energy: General features of large-scale perturbations, J. Cosmol. Astropart. Phys. 11 (2015) 029.

[14] D. Traykova, E. Bellini, P. G. Ferreira, C. García-García, J. Noller, and M. Zumalacárregui, Theoretical priors in scalar-tensor cosmologies: Shift-symmetric Horndeski models, Phys. Rev. D **104**, 083502 (2021).

[15] M. Raveri, L. Pogosian, K. Koyama, M. Martinelli, A. Silvestri, G.-B. Zhao, J. Li, S. Peirone, and A. Zucca, A joint reconstruction of dark energy and modified growth evolution, arXiv:2107.12990.

[16] A. Gómez-Valent and L. Amendola, H_0 from cosmic chronometers and type Ia supernovae, with Gaussian

processes and the novel weighted polynomial regression method, J. Cosmol. Astropart. Phys. 2018 (2018) 051.
[17] Y.-F. Cai, M. Khurshudyan, and E. N. Saridakis, Model-independent reconstruction of f(T) gravity from Gaussian processes, Astrophys. J. **888**, 62 (2020).
[18] K. Liao, A. Shafieloo, R. E. Keeley, and E. V. Linder, Determining model-independent H_0 and consistency tests, Astrophys. J. **895**, L29 (2020).
[19] A. Bonilla, S. Kumar, and R. C. Nunes, Measurements of H_0 and reconstruction of the dark energy properties from a model-independent joint analysis, Eur. Phys. J. C **81**, 127 (2021).
[20] D. Benisty, Quantifying the S_8 tension with the redshift space distortion data set, Phys. Dark Universe **31**, 100766 (2021).
[21] B. L'Huillier, A. Shafieloo, and H. Kim, Model-independent cosmological constraints from growth and expansion, Mon. Not. R. Astron. Soc. **476**, 3263 (2018).
[22] S. Vagnozzi, A. Loeb, and M. Moresco, Eppur è piatto? The cosmic chronometers take on spatial curvature and cosmic concordance, Astrophys. J. **908**, 84 (2021).
[23] Y. Yang and Y. Gong, Measurement on the cosmic curvature using the Gaussian process method, Mon. Not. R. Astron. Soc. **504**, 3092 (2021).
[24] A. Shafieloo, B. L'Huillier, and A. A. Starobinsky, Falsifying ΛCDM: Model-independent tests of the concordance model with eBOSS DR14Q and Pantheon, Phys. Rev. D **98**, 083526 (2018).
[25] F. Gerardi, M. Martinelli, and A. Silvestri, Reconstruction of the dark energy equation of state from latest data: The impact of theoretical priors, J. Cosmol. Astropart. Phys. 07 (2019) 042.
[26] M.-J. Zhang and H. Li, Gaussian processes reconstruction of dark energy from observational data, Eur. Phys. J. C **78**, 460 (2018).
[27] L. Perenon, M. Martinelli, S. Ilić, R. Maartens, M. Lochner, and C. Clarkson, Multi-tasking the growth of cosmological structures, Phys. Dark Universe **34**, 100898 (2021).
[28] J. Ruiz-Zapatero, C. García-García, D. Alonso, P. G. Ferreira, and R. D. P. Grumitt, Model-independent constraints on Ω_m and H(z) from the link between geometry and growth, Mon. Not. R. Astron. Soc. **512**, 1967 (2022).
[29] M. Seikel, C. Clarkson, and M. Smith, Reconstruction of dark energy and expansion dynamics using Gaussian processes, J. Cosmol. Astropart. Phys. 06 (2012) 036.
[30] N. Metropolis, A. W. Rosenbluth, M. N. Rosenbluth, A. H. Teller, and E. Teller, Equation of state calculations by fast computing machines, J. Chem. Phys. **21**, 1087 (1953).
[31] W. K. Hastings, Monte Carlo sampling methods using Markov chains and their applications, Biometrika **57**, 97 (1970).
[32] M. D. Hoffman and A. Gelman, The no-U-turn sampler: Adaptively setting path lengths in Hamiltonian Monte Carlo, arXiv:1111.4246.
[33] D. J. C. MacKay, *Information Theory, Inference & Learning Algorithms* (Cambridge University Press, Cambridge, England, 2002).
[34] M. Betancourt, A conceptual introduction to Hamiltonian Monte Carlo arXiv:1701.02434.
[35] J. Alsing and W. Handley, Nested sampling with any prior you like, Mon. Not. R. Astron. Soc. **505**, L95 (2021).
[36] J. Salvatier, T. Wiecki, and C. Fonnesbeck, Probabilistic programming in Python using PyMC, arXiv:1507.08050.
[37] C. C. Margossian, A review of automatic differentiation and its efficient implementation, WIREs **9**, e1305 (2018).
[38] R. Al-Rfou *et al.*, Theano: A Python framework for fast computation of mathematical expressions, arXiv:1605.02688.
[39] R. Jimenez and A. Loeb, Constraining cosmological parameters based on relative galaxy ages, Astrophys. J. **573**, 37 (2002).
[40] F. Hoyle and W. A. Fowler, Nucleosynthesis in supernovae, Astrophys. J. **132**, 565 (1960).
[41] S. A. Colgate and C. McKee, Early supernova luminosity, Astrophys. J. **157**, 623 (1969).
[42] M. M. Phillips, P. Lira, N. B. Suntzeff, R. A. Schommer, M. Hamuy, and J. Maza, The reddening-free decline rate versus luminosity relationship for type IA supernovae, Astron. J. **118**, 1766 (1999).
[43] W. L. Freedman, B. F. Madore, B. K. Gibson, L. Ferrarese, D. D. Kelson, S. Sakai, J. R. Mould, R. C. Kennicutt, H. C. Ford, J. A. Graham, J. P. Huchra, S. M. G. Hughes, G. D. Illingworth, L. M. Macri, and P. B. Stetson, Final results from the Hubble Space Telescope Key Project to measure the Hubble constant, Astrophys. J. **553**, 47 (2001).
[44] D. M. Scolnic *et al.*, The complete light-curve sample of spectroscopically confirmed SNe Ia from Pan-STARRS1 and cosmological constraints from the combined Pantheon sample, Astrophys. J. **859**, 101 (2018).
[45] P. Shah, P. Lemos, and O. Lahav, A buyer's guide to the Hubble constant, Astron. Astrophys. Rev. **29**, 9 (2021).
[46] P. J. E. Peebles and J. T. Yu, Primeval adiabatic perturbation in an expanding universe, Astrophys. J. **162**, 815 (1970).
[47] W. Hu and S. Dodelson, Cosmic microwave background anisotropies, Annu. Rev. Astron. Astrophys. **40**, 171 (2002).
[48] E. Komatsu *et al.*, Five-Year Wilkinson microwave anisotropy probe observations: Cosmological interpretation, Astrophys. J. Suppl. Ser. **180**, 330 (2009).
[49] M. R. Blanton *et al.*, Sloan Digital Sky Survey IV: Mapping the Milky Way, nearby galaxies, and the distant universe, Astron. J. **154**, 28 (2017).
[50] The SDSS-IV Extended Baryon Oscillation Spectroscopic Survey: Overview and early data, Astron. J. **151**, 44 (2016).
[51] N. Kaiser, Clustering in real space and in redshift space, Mon. Not. R. Astron. Soc. **227**, 1 (1987).
[52] S. Alam *et al.*, The clustering of galaxies in the completed SDSS-III Baryon Oscillation Spectroscopic Survey: Cosmological analysis of the DR12 galaxy sample, Mon. Not. R. Astron. Soc. **470**, 2617 (2017).
[53] J. Hou *et al.*, The completed SDSS-IV extended Baryon Oscillation Spectroscopic Survey: BAO and RSD measurements from anisotropic clustering analysis of the quasar sample in configuration space between redshift 0.8 and 2.2, Mon. Not. R. Astron. Soc. **500**, 1201 (2021),
[54] M. J. Drinkwater *et al.*, The WiggleZ Dark Energy Survey: Survey design and first data release, Mon. Not. R. Astron. Soc. **401**, 1429 (2010).

[55] B. E. Stahl, T. de Jaeger, S. S. Boruah, W. Zheng, A. V. Filippenko, and M. J. Hudson, Peculiar-velocity cosmology with Types Ia and II supernovae, Mon. Not. R. Astron. Soc. **505**, 2349 (2021).

[56] A. Font-Ribera, P. McDonald, N. Mostek, B. A. Reid, H.-J. Seo, and A. Slosar, DESI and other dark energy experiments in the era of neutrino mass measurements, J. Cosmol. Astropart. Phys. 2014 (2014) 023.

[57] S.-g. Hwang, B. L'Huillier, R. E. Keeley, M. J. Jee, and A. Shafieloo, How to use GP: Effects of the mean function and hyperparameter selection on Gaussian process regression, arXiv:2206.15081,

[58] C. R. Harris *et al.*, Array programming with NumPy, Nature (London) **585**, 357 (2020).

[59] J. D. Hunter, Matplotlib: A 2d graphics environment, Comput. Sci. Eng. **9**, 90 (2007).

[60] J. Lesgourgues, The Cosmic Linear Anisotropy Solving System (CLASS) I: Overview, arXiv:1104.2932.

[61] A. Lewis, GetDist: A Python package for analysing Monte Carlo samples, arXiv:1910.13970.

[62] S. Alam *et al.*, Completed SDSS-IV extended Baryon Oscillation Spectroscopic Survey: Cosmological implications from two decades of spectroscopic surveys at the Apache Point Observatory, Phys. Rev. D **103**, 083533 (2021).

[63] C. Blake *et al.*, The WiggleZ Dark Energy Survey: Joint measurements of the expansion and growth history at $z < 1$, Mon. Not. R. Astron. Soc. **425**, 405 (2012).

[64] A. Pezzotta *et al.*, The VIMOS Public Extragalactic Redshift Survey (VIPERS). The growth of structure at $0.5 < z < 1.2$ from redshift-space distortions in the clustering of the PDR-2 final sample, Astron. Astrophys. **604**, A33 (2017),

[65] F. Beutler, C. Blake, M. Colless, D. H. Jones, L. Staveley-Smith, G. B. Poole, L. Campbell, Q. Parker, W. Saunders, and F. Watson, The 6dF Galaxy Survey: $z \approx 0$ measurements of the growth rate and σ_8, Mon. Not. R. Astron. Soc. **423**, 3430 (2012).

[66] T. Okumura *et al.*, The Subaru FMOS galaxy redshift survey (FastSound). IV. New constraint on gravity theory from redshift space distortions at $z \sim 1.4$, Publ. ASJ **68**, 38 (2016).

[67] B. E. Stahl, T. de Jaeger, S. S. Boruah, W. Zheng, A. V. Filippenko, and M. J. Hudson, Peculiar-velocity cosmology with Types Ia and II supernovae, Mon. Not. R. Astron. Soc. **505**, 2349 (2021).

[68] A. G. Riess, S. Casertano, W. Yuan, J. B. Bowers, L. Macri, J. C. Zinn, and D. Scolnic, Cosmic distances calibrated to 1% precision with Gaia EDR3 parallaxes and Hubble Space Telescope photometry of 75 Milky Way cepheids confirm tension with ΛCDM, Astrophys. J. Lett. **908**, L6 (2021).

[69] D. J. Eisenstein and W. Hu, Baryonic features in the matter transfer function, Astrophys. J. **496**, 605 (1998).

[70] A. Aizpuru, R. Arjona, and S. Nesseris, Machine learning improved fits of the sound horizon at the baryon drag epoch, Phys. Rev. D **104**, 043521 (2021).